Variational Coupled Loads Analysis using the Hybrid Parametric Variation Method

Daniel C. Kammer, Paul Blelloch[1], and Joel Sills[2]

[1]ATA Engineering, Inc
13290 Evening Creek Drive S, San Diego, CA 92128

[2]NASA Johnson Space Center
2101 E. NASA Parkway, Houston, TX 77058

ABSTRACT

Time-domain coupled loads analysis (CLA) is used to determine the response of a launch vehicle and payload system to transient forces, such as liftoff, engine ignitions and shutdowns, jettison events, and atmospheric flight loads, such as buffet. CLA, using Hurty/Craig-Bampton (HCB) component models, is the accepted method for the establishment of design-level loads for launch systems. However, uncertainty in the component models flows into uncertainty in predicted system results. Uncertainty in the structural responses during launch is a significant concern because small variations in launch vehicle and payload mode shapes and their interactions can result in significant variations in system loads. Uncertainty quantification (UQ) is used to determine statistical bounds on prediction accuracy based on model uncertainty. In this paper uncertainty is treated at the HCB component-model level. In an effort to account for model uncertainties and statistically bound their effect on CLA predictions, this work combines CLA with UQ in a process termed variational coupled loads analysis (VCLA). The modeling of uncertainty using a parametric approach, in which input parameters are represented by random variables, is common, but its major drawback is the resulting uncertainty is limited to the form of the nominal model. Uncertainty in model form is one of the biggest contributors to uncertainty in complex built-up structures. Model-form uncertainty can be represented using a nonparametric approach based on random matrix theory (RMT). In this work, UQ is performed using the hybrid parametric variation (HPV) method, which combines parametric with nonparametric uncertainty at the HCB component model level. The HPV method requires the selection of dispersion values for the HCB fixed-interface (FI) eigenvalues, and the HCB mass and stiffness matrices. The dispersions are based upon component test-analysis modal correlation results. During VCLA, random component models are assembled into an ensemble of random systems using a Monte Carlo (MC) approach. CLA is applied to each of the ensemble members to produce an ensemble of system-level responses for statistical analysis. The proposed methodology is demonstrated through its application to a buffet loads analysis of NASA's Space Launch System (SLS) during the transonic regime fifty seconds after liftoff. Core stage (CS) section shears and moments are recovered, and statistics are computed.

Keywords: Uncertainty Quantification, Hurty/Craig-Bampton, Random Matrix, Model Form, Coupled Loads Analysis

ACRONYMS

CLA - coupled loads analysis
CS - core stage
DCGM - diagonal cross-generalized mass metric
DOF - degrees of freedom
FEM - finite element model
FI - fixed-interface

HCB - Hurty/Craig-Bampton
HPV - hybrid parametric variation
ICPS - interim cryogenic propulsion stage
ISPE - integrated spacecraft payload element
LSRB - left solid rocket booster
LVSA - launch vehicle stage adapter
MC - Monte Carlo
ME - maximum entropy
MEM - modal effective mass
MUF - model uncertainty factor
MPCV - Multi-Purpose Crew Vehicle
MSA - MPCV stage adapter
NPV - nonparametric variation
OTM - output transformation matrix
PDF - probability distribution function
RINU - replaceable inertial navigation unit
RMS - root mean square
RMT - random matrix theory
RSRB - right solid rocket booster
SLS - Space Launch System
UQ - uncertainty quantification
VCLA - variational coupled loads analysis

INTRODUCTION

Uncertainty in structural responses during launch is a significant concern in the development of spacecraft and launch vehicles. Small variations in launch vehicle and payload mode shapes and their interactions can result in significant variations in system loads. Time-domain coupled loads analysis (CLA) is used to determine the response of a launch vehicle and payload system to transient forces, such as liftoff, engine ignitions and shutdowns, jettison events, and atmospheric flight loads. Atmospheric flight loads include static-aeroelastic, turbulence/gust, and buffet loads. CLA, using Hurty/Craig-Bampton (HCB) [1] component models, is the accepted method for the establishment of design-level loads for launch systems, but it is an expensive and time-consuming process that is performed a limited number of times using a sequence of increasingly more accurate system models. Ideally, a modal test of the integrated system is performed, and the resulting test-correlated system model is used in the final CLA. However, in many cases, an integrated-system test is not practical, so the accuracy of the system model is dependent on the accuracy of component models that are correlated and updated using component test results. Unfortunately, component test configurations are rarely, if ever, the same as component flight configurations, resulting in uncertainty in the component and, thus, system models. In addition, as a program advances, inevitable increasing cost and time constraints begin to limit the number of component tests that are actually performed before launch, which, again, increases the amount of uncertainty in the models and CLA results. In an effort to account for model uncertainties and their effect on CLA predictions, CLA sensitivity analyses could be performed, but due to the high cost of multiple CLAs, this has been impractical and typically not done. Another standard practice is to apply model uncertainty factors (MUF) to the predicted CLA load results. This is simple, but the MUF approach is not based on test results of the specific system it is being applied to, and such a blanket approach may be needlessly conservative in some instances, but unconservative in others.

Uncertainty quantification (UQ) is used to determine statistical bounds on prediction accuracy based on model uncertainty. In the case of NASA's Space Launch System (SLS), uncertainty is modeled at the HCB component-model level because it has the most direct link to modal test results. This work combines CLA with UQ in a process termed variational coupled loads analysis (VCLA) [2]. In the past, VCLA has not been feasible due to computational expense. But due to advances in computational speed, software, and mathematical approaches, VCLA is beginning to be practical, provided that care is taken in how the variations are modeled. The modeling of uncertainty using a parametric approach, in which finite element model

(FEM) input parameters are represented by random variables, is common. The major drawback is that the resulting uncertainty is limited to the form of the nominal model. Uncertainty in model form is one of the biggest contributors to uncertainty in complex built-up structures. One way to treat model-form uncertainty is to use a nonparametric approach based on random matrix theory (RMT). In this work, UQ is performed using the hybrid parametric variation (HPV) [3] method, which combines parametric with nonparametric uncertainty at the HCB component-model level. The HPV method requires the selection of dispersion values for the HCB fixed-interface eigenvalues, and the HCB mass and stiffness matrices. The dispersions are based upon component test-analysis modal correlation results. During VCLA, random component models are assembled into an ensemble of random systems using a Monte Carlo (MC) approach. CLA is applied to each of the systems to produce an ensemble of system-level responses for statistical analysis. The proposed methodology is demonstrated through its application to a buffet loads analysis of the SLS during the transonic regime at 50 seconds after liftoff. Core stage (CS) section shears and moments are recovered, and statistics, such as P99/90 non-exceedance values, are computed.

THEORY

The SLS consists of components that are assembled into the launch vehicle. In order to predict system performance, FEMs of the components are developed, reduced to HCB representations, and assembled to represent different phases of flight. There is always uncertainty in every model, which flows into uncertainty in predicted system results. For the SLS, it is natural to treat the model uncertainty at the HCB component-model level. The HCB component-model displacement vector is given by $u_{HCB} = \{x_t^T \quad q^T\}^T$, where x_t is the vector of physical displacements at the component interface, and q is the vector of generalized coordinates associated with the component fixed-interface (FI) modes. Given the assumption that the FI modes are mass normalized, the corresponding HCB mass and stiffness matrices have the form

$$M_{HCB} = \begin{bmatrix} M_S & M_{tq} \\ M_{tq}^T & I \end{bmatrix} \qquad K_{HCB} = \begin{bmatrix} K_S & 0 \\ 0 & \lambda \end{bmatrix} \tag{1}$$

in which M_S and K_S are the component physical mass and stiffness matrices statically reduced to the interface, M_{tq} is the mass coupling between the interface and the fixed-interface modes, I is an identity matrix, and λ is a diagonal matrix of the FI mode eigenvalues. Details of the HCB component-model derivation can be found in reference [1].

In this work, uncertainty in the component HCB representations is quantified using the HPV approach, which combines parametric with nonparametric uncertainty. Purely parametric uncertainty approaches are the most common in the structural dynamics community. Component parameters that are inputs to the FEM, such as Young’s modulus, mass density, geometric properties, etc., are modeled as random variables. Parametric uncertainty can be propagated into the system response using a method such as stochastic finite element analysis [4]. The advantage of the parametric approach is that each random set of model parameters represents a specific random FEM. However, there are disadvantages associated with the parametric method: it can be very time consuming, there are an infinite number of ways to parameterize the model, and the selected parameter probability distributions are generally not available. The most significant drawback is that the uncertainty represented is limited to the form of the nominal FEM. It is known that most errors in a FEM stem from modeling assumptions or model-form errors, not parametric errors. Therefore, in practice, the parameter changes are merely surrogates for the actual model errors. In the case of HPV, the HCB components are parameterized in terms of the FI eigenvalues, not the inputs to the original FEM. While there is not a simple direct connection between the random FI eigenvalues and a random component FEM, there is a direct connection to the corresponding random HCB component.

Uncertainty in model form is likely the largest contributor to uncertainty in complex built-up structures, as it cannot be directly represented by model parameters and thus cannot be included in a parametric approach. Familiar examples include unmodeled nonlinearities, errors in component joint models, etc. Instead, model-form uncertainty can be modeled using random matrix theory (RMT), where a probability distribution is developed for the matrix ensemble of interest. RMT was introduced and developed in mathematical statistics by Wishart [5], and more recently, Soize [6] [7] developed a nonparametric variation (NPV) approach to represent model-form uncertainty in structural dynamics applications. Soize’s approach was extended by Adhikari [8] [9] using Wishart distributions to model random structural mass, damping, and stiffness matrices. The nonparametric matrix-based approach to representing structural uncertainty has been used extensively in aeronautics and aerospace engineering applications [10] [11] [12].

Soize [7] employed the maximum entropy (ME) principle to derive the positive and positive-semidefinite ensembles SE^{+} and SE^{+0} that follow a matrix variate gamma distribution and are capable of representing random structural matrices. This means that the matrices in the ensembles are real and symmetric and possess the appropriate sign definiteness to represent structural mass, stiffness, or damping matrices. As the dimension of the random matrix *n* increases, the matrix variate gamma distribution converges to a matrix variate Wishart distribution. In structural dynamics applications, the matrix dimensions are usually sufficient to give a negligible difference between the two distributions. In letting ensemble member random matrix *G* be any of the random mass, stiffness, or damping matrices, it is assumed in this work that *G* follows a matrix variate Wishart distribution, $G \sim W_n(p, \Sigma)$. In general, a Wishart distribution with parameters *p* and Σ can be thought of as the sum of the outer product of *p* independent random vectors X_i all having a multivariate normal distribution with zero mean and covariance matrix Σ. Parameter *p* is sometimes called the shape parameter. The random matrix *G* can be written as

$$G = \sum_{i=1}^{p} X_i X_i^T \qquad X_i \sim N_n(0, \Sigma) \tag{2}$$

where the expected value is given by

$$E(G) = \bar{G} = p\Sigma \tag{3}$$

The dispersion or normalized standard deviation of the random matrix *G* is defined by the relation

$$\delta_G^2 = \frac{E\left(\|G - \bar{G}\|_F^2\right)}{E\left(\|\bar{G}\|_F^2\right)} \tag{4}$$

in which $\|*\|_F^2$ is the Frobenius norm squared, or $\mathrm{trace}(*^T *)$. It can be shown that Eq. (4) reduces to the expression

$$\delta_G^2 = \frac{1}{p}\left[1 + \frac{\left(tr(\bar{G})\right)^2}{tr(\bar{G}^T \bar{G})}\right] = \frac{1}{p}\left[1 + \gamma_G\right] \tag{5}$$

where $\gamma_G = \frac{\left(tr(\bar{G})\right)^2}{tr(\bar{G}^T \bar{G})}$ can be thought of as a measure of the magnitude of the matrix. The uncertainty in the random matrix *G* is dictated by the shape parameter *p*, the number of inner products in Eq. (2). The larger the value of *p*, the smaller the dispersion δ_G. There may be instances when it is desirable to have the same amount of uncertainty in two or more substructures. Suppose G_1 and G_2 represent structural matrices, such as stiffness, from two different system components. In order to have equivalent uncertainty in the two matrices, the shape parameter *p* must be the same for both ensembles. However, Eq. (5) shows that even if $p_1 = p_2 = p$, the dispersion values are not the same in general, $\delta_{G_1}^2 \neq \delta_{G_2}^2$, unless $\gamma_1 = \gamma_2$. A more useful definition of matrix dispersion is the normalized dispersion

$$\delta_{G_n} = \frac{\delta_{G_1}}{\sqrt{1+\gamma_1}} = \frac{\delta_{G_2}}{\sqrt{1+\gamma_2}} = \frac{1}{\sqrt{p}} \tag{6}$$

which is independent of the matrix magnitude γ_G. It is important to realize, however, that just because two components have the same normalized dispersion, this does not mean that they will have the same uncertainty relative to a specific metric used to quantify component uncertainty, such as modal parameter uncertainty. Where the normalized dispersion is small, the modal statistics of the two components tend to be close, but as the normalized dispersion increases, the modal statistics for the two components become more disparate due to nonlinearity. Therefore, while Eq. (6) can be used to initially set a component matrix dispersion, it should ultimately be checked and adjusted based on the specific metric being used to quantify component uncertainty.

Adhikari [8] referred to the random matrix method developed by Soize [6] [7] as Method 1. The Wishart parameters are selected as p and $\Sigma = G_o/p$ where G_o is the nominal value of *G*. The mean of the distribution is given by Eq. (3) as $\bar{G} =$

$p\Sigma = p(G_o/p) = G_o$. Therefore, Method 1 preserves the nominal matrix as the mean of the ensemble. In general, the nominal matrix can be decomposed in the form

$$G_o = LL^T \tag{7}$$

In the case of a positive definite matrix, this would just be the Cholesky decomposition. Let $(n \times p)$ matrix X be given by

$$X = \begin{bmatrix} x_1 & x_2 \cdots x_p \end{bmatrix} \tag{8}$$

in which x_i is an $(n \times 1)$ column vector containing standard random normal variables such that $x_i \sim N_n(0, I_n)$. Note that $p \geq n$ must be satisfied in order for G to be full rank. An ensemble member $G \sim W_n(p, G_o/p)$ can then be generated for MC analysis using the expression

$$G = \frac{1}{p} LXX^T L^T \tag{9}$$

It has been found that ensembles of random component mass matrices are best represented using Method 1. Adhikari [8] noted that Method 1 does not maintain the inverse of the mean matrix as the mean of the inverse; that is

$$E(G^{-1}) \neq [E(G)]^{-1} = \bar{G}^{-1} \tag{10}$$

In some cases, the two can be vastly different, which is clearly not physically realistic. Instead, he proposed Method 3, in which the Wishart parameters are selected as p and $\Sigma = G_o/\theta$ where

$$\theta = \frac{1}{\delta_G^2}[1 + \gamma_G] - (n+1) \tag{11}$$

An ensemble member $G \sim W_n(p, G_o/\theta)$ can then be generated using the relation

$$G = \frac{1}{\theta} LXX^T L^T \tag{12}$$

In this case, the inverse of the mean matrix is preserved as the mean of the ensemble inverses, where the mean matrix is now given by

$$\bar{G} = p\Sigma = p(G_o/\theta) = \frac{p}{\theta} G_o \tag{13}$$

In Method 3, the dispersion defined in Eq. (4) is now calculated with respect to the mean given in Eq. (13), while Eqs. (5) and (6) still hold. It has been determined that ensembles of random component stiffness matrices are best represented using Method 3. Therefore, the nonparametric portion of the HPV method is based on a Method 1 randomization of the component mass matrix and a Method 3 randomization of the component stiffness matrix. In this approach, the random component mass and stiffness matrices are assumed to be independent.

Note that the Wishart matrix uncertainty model results in uncertainty both in mode shapes and in frequencies. However, MC simulation and analysis has shown that component mode shapes tend to be sensitive to the nonparametric matrix randomization provided by Methods 1 and 3, but the corresponding modal frequencies tend to be relatively insensitive. Therefore, a parametric component of uncertainty was added to the HPV approach in which the eigenvalues of the FI modes in the component HCB representation are also assumed to be random variables. ME is also used to derive the probability distribution function (PDF) for the HCB FI eigenvalues. The ME principle produces a PDF based solely on the available information, and in this case, there are two pieces of information available: First, the i^{th} random eigenvalue must be strictly positive. Second, the expected value of the random eigenvalue is given by the nominal value. The application of ME yields a gamma distribution, $\lambda_{ri} \sim G(k_i, \theta_i)$, where the shape parameter k_i and the scale parameter θ_i are given by $k_i = \delta_i^{-2}$ and $\theta_i = \lambda_i \delta_i^2$, in which δ_i is the corresponding coefficient of variation, or dispersion [13].

The FI eigenvalues are then independent random parameters within the HCB component stiffness matrix. The validity and impact of this assumption can be determined by considering only the FI component of the HCB substructure representation. The corresponding equation of motion in physical coordinates is given by

$$M_{oo}\ddot{u}_o + K_{oo}u_o = F_o \tag{14}$$

while the equation of motion in FI modal coordinates is

$$I\ddot{q} + \lambda q = \phi^T F_o \tag{15}$$

where the modal stiffness λ is a diagonal matrix of FI modal eigenvalues from Eq. (1). The modal stiffness is given by

$$\lambda = \phi^T K_{oo}\phi \tag{16}$$

The physical stiffness can be recovered by pre-multiplying Eq. (16) by $M_{oo}\phi$ and post-multiplying by $\phi^T M_{oo}$ producing

$$M_{oo}\phi\phi^T K_{oo}\phi\phi^T M_{oo} = M_{oo}\phi\lambda\phi^T M_{oo} \tag{17}$$

If all FI modes are retained, then $\phi\phi^T M_{oo} = I$. In considering only the i^{th} mode, Eq. (17) becomes

$$K_{ooi} = P_i^T K_{oo} P_i = M_{oo}\phi_i\lambda_i\phi_i^T M_{oo} \tag{18}$$

where $P_i = \phi_i\phi_i^T M_{oo}$ is an oblique projector [14] onto the column space spanned by the i^{th} FI mode and K_{ooi} is the contribution of the i^{th} FI mode to the FI physical stiffness matrix. The physical stiffness can then be expressed as

$$K_{oo} = \sum_{i=1}^{n_o} K_{ooi} = \sum_{i=1}^{n_o} \lambda_i (M_{oo}\phi_i\phi_i^T M_{oo}) \tag{19}$$

Therefore, the randomized physical stiffness matrix that corresponds to the randomized FI eigenvalues λ_{ri} is given by

$$K_{oor} = \sum_{i=1}^{n_o} \alpha_i K_{ooi} = \sum_{i=1}^{n_o} \alpha_i\lambda_i (M_{oo}\phi_i\phi_i^T M_{oo}) = \sum_{i=1}^{n} \lambda_{ri} (M_{oo}\phi_i\phi_i^T M_{oo}) \tag{20}$$

where α_i is a random variable selected from a gamma distribution with a mean value of 1.0 and n_o is the number of FI modes. Equation (20) indicates that the parameterization of the FI stiffness in modal space using the eigenvalues λ_i corresponds to the parameterization of the FI stiffness in physical space using the matrices K_{ooi}. The randomized stiffness parameters $K_{oori} = \alpha_i K_{ooi}$ are independent of one another, meaning that changing the i^{th} stiffness parameter has no impact on any of the other stiffness parameters.

In summary, the FI eigenvalue parameterization used in the HPV method is equivalent to a parameterization within physical FI space where the stiffness components for the individual modes are scaled by n_o independent random parameters. The resulting sum produces a random physical stiffness matrix that preserves the nominal FI modes, but the generalized stiffness or eigenvalues vary. While the HPV FI eigenvalue parameterization preserves the model form of the HCB representation stiffness matrix, it does not preserve the model form of the physical FI stiffness matrix. Therefore, the variation of the HCB FI eigenvalues is a purely parametric variation with respect to the HCB representation, but it is not a purely parametric variation with respect to the physical stiffness partition K_{oo}, meaning that it also results in model-form uncertainty. Also, if the corresponding random HCB stiffness matrix in its entirety is back transformed into physical coordinates, then not only is the K_{oo} partition randomized as discussed above, but the K_{aa} and K_{ao} partitions, corresponding to the interface DOF, are also randomized such that the sign-definiteness and the rigid body modes are preserved. The fact that this parameterization affects the FI eigenvalues but not the FI mode shapes allows it to be paired with the NPV method to produce a maximal impact on the HCB frequencies and a minimal impact on the HCB mode shapes. Therefore, the HPV approach provides the capability to almost independently adjust the uncertainty in the component frequencies and mode shapes, by adjusting the dispersion of the FI eigenvalues vs. the dispersions of the HCB mass and stiffness matrices. It is important to emphasize that this parameterization is not equivalent to the usual model input parameterization of the FEM.

In contrast, if all of the random FI eigenvalues are varied in unison, such they are no longer independent, but perfectly correlated, then the random FI partition in physical space is given by

$$K_{oor} = \sum_{i=1}^{n} \alpha_i K_{ooi} = \alpha \sum_{i=1}^{n} K_{ooi} = \alpha K_{oo} \tag{21}$$

which is just a random scaling of the nominal stiffness. This randomization of the FI eigenvalues then preserves the physical stiffness model form as well as the model form of the HCB stiffness matrix. As in the previous case, if the corresponding random HCB stiffness matrix is transformed back into physical coordinates, then the entire physical stiffness matrix is a scaled version of the nominal physical stiffness with the same random scale factor α, and the model form is still preserved.

During each iteration in an MC analysis, a random draw of HCB FI eigenvalues is selected to generate a random HCB component stiffness matrix as described. The mean of this ensemble would just be the nominal HCB stiffness matrix. However, for each iteration, the parametrically randomized HCB stiffness is treated as the nominal matrix, and Method 3 is applied to provide model-form uncertainty on top of the FI eigenvalue parametric uncertainty. This is analogous to the approach proposed by Capiez-Lernout [10] for separating parametric and nonparametric uncertainty. Component frequency uncertainty can be based on component test-analysis frequency correlation, and the nonparametric mass and stiffness dispersion can be based on the corresponding orthogonality and cross-orthogonality results.

The component slosh modes are likely to have much less uncertainty associated with them. In addition, there may be times when the component mass must be randomized while the rigid body mass is preserved. A special methodology has been developed within the HPV method to preserve the component slosh modes and rigid body mass when desired; the same methodology can be applied to any subset of the component modes. When the nominal matrix is positive semidefinite, such as in the case of an SLS flight component that has rigid body modes and a positive semidefinite stiffness matrix, special steps must be taken to decompose the nominal HCB stiffness matrix for subsequent randomization using Method 3 and Eq. (12). As in the case of component mass randomization, the slosh mode stiffness must be preserved. In addition, the rigid body stiffness must be preserved as the null matrix. Details of the methodology's implementation within the HPV framework are given in reference [3].

SELECTION OF COMPONENT EIGENVALUE AND STIFFNESS MATRIX DISPERSION VALUES

The HPV approach for modeling component uncertainty requires the selection of dispersion values for the HCB component FI eigenvalues, mass matrix, and stiffness matrix. Ideally, these dispersion values are selected for each component based on component modal test results. This is because test-analysis modal correlation metrics are used to determine the dispersions. Test-analysis frequency error is used to identify the HCB FI eigenvalue uncertainties, but one of the biggest challenges in the propagation of component test-analysis frequency error into uncertainty in the HCB flight configuration FI modes is that the component test configuration and the component flight configuration boundary conditions and/or hardware are almost never the same. Because of this, it is difficult to match test configuration modes with flight configuration FI modes. The boundary condition mismatch can be alleviated using a mixed-boundary approach. In general, the HCB flight configuration FI modes will be over-constrained when compared to the test configuration modes. Therefore, the HCB stiffness matrix in Eq. (1) can be written as

$$K_{HCB} = \begin{bmatrix} K_S & 0 \\ 0 & \lambda \end{bmatrix} = \begin{bmatrix} K_{cc} & K_{cb} & 0 \\ K_{bc} & K_{bb} & 0 \\ 0 & 0 & \lambda \end{bmatrix} \tag{22}$$

where the HCB flight configuration set of boundary degrees of freedom (DOF) have been divided into two subsets: the *c*-set contains all DOF that are free in the component test configuration, and the *b*-set contains the DOF that are constrained in the component test configuration. When the HCB flight configuration is constrained at the test configuration interface DOF (*b*-set), it produces the mass and stiffness matrices

$$M_C = \begin{bmatrix} M_{cc} & M_{cq} \\ M_{qc} & M_{qq} \end{bmatrix} \qquad K_C = \begin{bmatrix} K_{cc} & 0 \\ 0 & \lambda \end{bmatrix} \tag{23}$$

with corresponding eigenvalues λ_C and mass normalized eigenvectors $\phi_C = \begin{bmatrix}\phi_{cc}^T & \phi_{cq}^T\end{bmatrix}^T$. These eigenvalues and eigenvectors are consistent with the boundary conditions of the test configuration modes used in the component test-analysis correlation. Error or uncertainty in the analytical test configuration eigenvalues can be much more easily mapped onto uncertainty $\Delta\lambda_C$ in the eigenvalues of the system in Eq. (23). The HCB representation of the component using λ_C and ϕ_C as FI modal properties has the stiffness matrix and corresponding displacement vector given by

$$K_B = \begin{bmatrix} K_{Sb} & 0 \\ 0 & \lambda_C \end{bmatrix} \qquad u_B = \{x_b^T \quad q_C^T\}^T \tag{24}$$

where K_{Sb} is K_S statically reduced to the *b*-set, x_b is the physical displacement of the *b*-set, and q_C are the modal coordinates of the FI modes with the *c*-set free. The transformation between displacement vector u_B and the original HCB displacement vector u_{HCB} is given by

$$u_{HCB} = \begin{Bmatrix} x_c \\ x_b \\ q \end{Bmatrix} = \begin{bmatrix} \psi & \phi_{cc} \\ I & 0 \\ 0 & \phi_{cq} \end{bmatrix} \begin{Bmatrix} x_b \\ q_C \end{Bmatrix} = T u_B \tag{25}$$

The relation between K_B and K_{HCB} is then

$$K_B = T^T K_{HCB} T \tag{26}$$

The test configuration HCB FI eigenvalues λ_C can be randomized (λ_{Cr}) based upon the component test-analysis correlation results, and the uncertainty can be propagated into the random flight configuration HCB component stiffness (K_{HCBr}) using the expression

$$K_{HCBr} = T^{-T} K_{Br} T^{-1} = T^{-T} \begin{bmatrix} K_{Sb} & 0 \\ 0 & \lambda_{Cr} \end{bmatrix} T^{-1} \tag{27}$$

Details of the procedure used to assign the uncertainty to the eigenvalues λ_C are discussed in the following section. Reference [3] details a procedure for identifying the HCB mass matrix dispersion based upon the component test mode self-orthogonality matrix. Alternatively, the mass matrix dispersion could be based on engineering judgment, past experience, and historical results. In this work, it is assumed that the mass representation of the components is accurate, so the mass matrix is not dispersed. Once the eigenvalue dispersions have been identified, test-analysis cross-orthogonality is used to identify the dispersion of the component stiffness matrix. In this case, the root mean square (RMS) diagonal value of the component test-analysis cross-orthogonality matrix, referred to as the diagonal cross-generalized mass (DCGM), is used as the metric. For this, a series of MC analyses is performed in which the HCB stiffness matrix dispersion value is swept over a range, and the most probable value of DCGM is computed for each MC analysis. The goal is to select the stiffness dispersion value that gives the most probable DCGM value that is equal to the test result. Details of the identification procedure are discussed in the following section and in reference [3].

NOMINAL ICPS/LVSA BASED ON ISPE CONFIGURATION 3

Dispersion values for the combined nominal interim cryogenic propulsion stage (ICPS)/ launch vehicle stage adapter (LVSA) HCB components are based on the integrated spacecraft payload element (ISPE) configuration 3 modal test-analysis correlation results. The FEM representation of ISPE configuration 3 is shown in Figure 1. There are eleven FEM target modes matched to eleven of nineteen test modes. Only these target modes are considered in this analysis, because the other eight modes are dominated by the MPCV stage adapter (MSA)/Multi-Purpose Crew Vehicle (MPCV) simulator, which is not part of the ICPS/LVSA component. The test-analysis frequency correlation results are listed in Table 1. The nominal model accurately predicts the first bending test mode frequencies. This is consistent with the static test results, which showed good agreement between the nominal model and the test results for overall bending and axial stiffness. Only one second-order bending test mode was identified in the test data, and no axial modes were identified. The nominal model does a poor job of predicting the second-order bending test mode frequency, and the LVSA shell test mode frequencies are even less accurately predicted. Note that the frequency error is calculated relative to the nominal FEM frequency rather than the test; this is done because the uncertainty analysis is performed relative to the FEM HCB representation. As mentioned, the SLS HCB flight components and the test components do not match in most cases. In the case of the ICPS/LVSA HCB flight component, there is no MSA nor MPCV simulator. In addition, the ISPE configuration 3 is not tested in the HCB flight configuration. At the time of this writing, the mixed-boundary approach discussed above has not yet been applied to the ICPS/LVSA HCB flight component. Instead, the test configuration modal frequency uncertainties are mapped directly onto the ICPS/LVSA HCB flight component FI modes. It is assumed that the component test correlation results can be used as an indicator of what level of uncertainty is expected in the corresponding HCB component model.

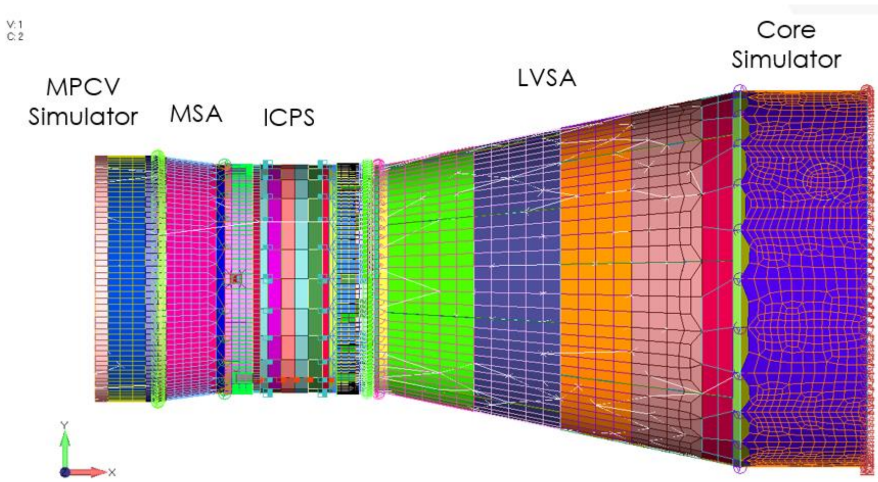

Fig. 1 ISPE configuration 3 FEM representation

Table 1 Test-analysis frequency error for ISPE configuration 3 nominal model

Test Mode	Pretest Mode	Error	Posttest Mode	Error	Description
1	6	−0.16%	6	−0.89%	First bending
2	5	−1.94%	5	−2.70%	First bending
3	9	10.13%	7	1.43%	LVSA shell ND 5
4	10	9.95%	8	1.23%	LVSA shell ND 5
5	11	7.21%	9	3.96%	LVSA shell ND 4
6	12	6.97%	10	3.50%	LVSA shell ND 4
9	14	12.90%	14	−0.23%	LVSA shell ND 6
10	13	12.60%	13	−0.57%	LVSA shell ND 6
14	24	15.29%	20	−0.01%	LVSA shell ND 7
15	23	14.98%	19	−0.33%	LVSA shell ND 7
19	22	−8.63%	24	−4.72%	Second bending

The first element of uncertainty to be specified is the dispersion of the 33 non-slosh FI modal frequencies for the HCB flight component. These modes have the base of the LVSA and the top of the ICPS at the MSA interface constrained, whereas during the test, the base of the LVSA is attached to the core simulator, and the top of the ICPS is attached to the MSA/MPCV simulator. Test-analysis frequency error is mapped onto the FI modes using modal effective mass (MEM). The nominal FEM ISPE configuration 3 MEM is dominated by the fundamental bending and axial modes, and to a lesser extent, the second-order bending modes. The LVSA shell modes have little or no MEM. Based on MEM, the HCB FI modes are placed in three different bins of frequency uncertainty. Bin 1, associated with the FEM configuration 3 first bending pair, is assigned a frequency dispersion of 1.39%, corresponding to the RMS error in the prediction of the first bending configuration 3 test mode pair frequencies. The modal frequencies are assumed to follow the gamma distribution described previously. Bin 2 has a frequency dispersion of 9.01%, corresponding to the test-analysis frequency error of the second-order bending configuration 3 mode. FI modes that have little or no MEM, analogous to the LVSA shell test modes, are assigned to bin 3 with a frequency dispersion of 10.91%, corresponding to the RMS frequency error in the configuration 3 LVSA shell modes.

Once the FI eigenvalue uncertainty is applied, the dispersion of the stiffness matrix is determined by computation of the DCGM metric based on cross-orthogonality, which is the RMS value of the diagonal after modes are matched and resorted accordingly. Based on the nominal ISPE configuration 3 cross-orthogonality matrix for the eleven target modes, the dispersion metric has the value DCGM = 90.44. The goal is to select a stiffness dispersion value for the MC analysis such that the test-based metric value is the most probable. The MC analysis is based on the first 37 nominal HCB elastic non-slosh modes and 3000 ensemble members. The selected FI eigenvalue uncertainties are applied, and then a series of MC analyses are performed with stiffness dispersion swept over a range of values. A stiffness dispersion of 7%, which corresponds to a normalized dispersion of 0.85%, produces the most probable DCGM value that agrees with the test value.

UPDATED ICPS/LVSA BASED ON ISPE CONFIGURATION 3

A posttest correlation was performed to update the ISPE configuration 3 FEM; thus, dispersion values for the updated ICPS/LVSA HCB component are based on the updated ISPE configuration 3 FEM. Like the nominal model analysis, there are eleven FEM target modes matched to eleven of nineteen test modes. The test-analysis frequency correlation results are also listed in Table 1. Note that the frequency error for the LVSA shell modes and the second-order bending modes have been dramatically reduced. There are now 243 HCB FI non-slosh modes in the updated ICPS/LVSA fifty-seconds-of-ascent HCB component. The FI MEM is calculated and the same three-bin uncertainty assignment strategy is applied. Bin 1 is assigned a frequency dispersion of 2.04%, corresponding to the RMS error in the prediction of the first bending test mode pair. Bin 2 is assigned a frequency dispersion of 4.83%, corresponding to the test-analysis frequency error of the second-order bending test mode. As in the nominal model analysis, the remaining FI modes have little or no MEM, analogous to the LVSA shell test modes. Therefore, these FI modes are assigned to bin 3 with a frequency dispersion of 1.97%, corresponding to the RMS frequency error in the configuration 3 LVSA shell modes.

Based on the updated ISPE configuration 3 cross-orthogonality matrix for the eleven target modes, the dispersion metric has the test value DCGM = 95.43. The selected FI eigenvalue uncertainties were applied, and then a series of MC analyses were performed with stiffness dispersion swept over a range of values. In this case, the MC analysis was based on the first 35 nominal HCB elastic non-slosh modes to about 20 Hz and 3000 ensemble members. The DCGM metric was computed for each ensemble member cross-orthogonality matrix. The stiffness dispersion that produced the most probable DCGM metric that was in greatest agreement with the test value was 9%, which corresponds to a normalized dispersion of 1.01%. Further details on the procedure used to assign ICPS/LVSA HCB FI frequency and stiffness matrix dispersions for the pretest and updated models can be found in reference [3].

PROPAGATION OF UNCERTAINTY INTO RESPONSE TO BUFFET LOADS

Buffet loads are forces on the system flight vehicle caused by the interactions between separated flow turbulence, attached boundary layer turbulence, and shock wave oscillations [15]. A buffet loads analysis can be performed in either the frequency or the time domain. The SLS program uses the time-domain approach. The forcing function time histories are generated from wind tunnel tests of scale models [16]. The time domain has several advantages over the frequency domain: time histories of various loads can be combined, and the phasing is automatically correct; the size of the problem is reduced because a frequency-domain analysis requires force cross-spectra; and the response time histories can be used directly in subsequent MC analysis [15].

The HPV approach for uncertainty quantification and propagation was applied to the SLS fifty-seconds-of-ascent (Ascent 50) configuration with buffet loads in the transonic regime at Mach 0.9 and 0.0 degrees of pitch and roll. The corresponding CLA model assembled from HCB components has over 12,000 DOF. This proved to be too large for VCLA, but through the judicious combination of interfaces, selection of residual vectors, elimination of internal DOF, and reduction in component mode frequency cutoff, the size of the assembled model was reduced to 4,102 DOF, which is an acceptable size for VCLA. It requires approximately 33 s on a desktop computer to perform one MC iteration, which makes it feasible to run about 1000 iterations overnight. The SLS HCB components contained FI modes to 65 Hz plus 6 modal truncation vectors (MTVs) for each component interface. In addition, there is a residual vector for each buffet force application DOF, due to the fact that they are interior to the components. One percent modal damping was used for system modes up to 20 Hz, and 2% modal damping was used for system modes above 20 Hz. The buffet loads were applied to core and solid rocket booster (SRB) centerline nodes for 100 s with system modes to 50 Hz and system-level residual flexibility. Response due to buffet loading involves system oscillations with relatively small rigid body motion, so the aerodynamic damping and stiffness can be conservatively neglected [15]. The appropriate equation of motion in system modal coordinates is then given by

$$I\ddot{q}_S + 2\zeta_S\omega_S\dot{q}_S + \omega_S^2 q_S = \phi_S^T F_B \tag{28}$$

where q_S is a vector of system generalized coordinates, ζ_S is a diagonal matrix of modal damping, ω_S is a diagonal matrix of system natural frequencies, and F_B is the vector of buffet forces. In this application, it is assumed that the buffet loads are zero mean and Gaussian, and that the time histories are long enough that the RMS values have converged. Figure 2 illustrates the RMS buffet forces per unit length applied along the SRB and CS centerline nodes.

CS section loads were recovered using displacement and acceleration output transformation matrices (OTM), which were transformed to the reduced model used in the UQ analysis. Nominal model CS RMS section loads are shown in Figure 3. The CS sections loads will also be zero mean Gaussian, and it is assumed that there is infinite data. For a narrowband response to zero-mean Gaussian inputs, the peaks and the corresponding envelope function will follow a Rayleigh distribution [17]. The quantile function, or inverse of the cumulative distribution function, Q_P for a Rayleigh distribution is given by the expression

$$Q_P = \sigma\sqrt{-2\ln(1-P)} = \sigma\xi_P \tag{29}$$

For 99% enclosure, $P = 0.99$, and the P99 response value is given by

$$x_{.99} = \sigma\sqrt{-2\ln(1-.99)} = \xi_{.99}\sigma = (3.03485)\sigma \tag{30}$$

where σ is the Rayleigh distribution shape parameter, which is equivalent to the RMS value of the time-domain response x. Therefore, the P99 value for the response can be determined using

$$x_{.99} = \xi_{.99}x_{RMS} \tag{31}$$

In the case of a more broadband response like the current situation, the Rayleigh assumption and Eq. (31) provide a conservative estimate of the P99 response. Unfortunately, the actual buffet loads that are applied are not quite Gaussian, and the resulting CS section load envelope functions [17] are not quite Rayleigh, therefore Eq. (31) does not bound the actual P99 peak value. Alternatively, the .99 quantile of the envelope function $\tilde{x}$ could be computed. The P99 value based on the envelope function will always give bounding results regardless of whether the time histories are zero mean Gaussian. However, the current variational buffet loads analysis is for demonstration purposes only, so for simplicity, the Rayleigh approximation in Eq. (31) is used to compute P99 CS section loads. Further details on computing P99 peak response can be found in reference [17].

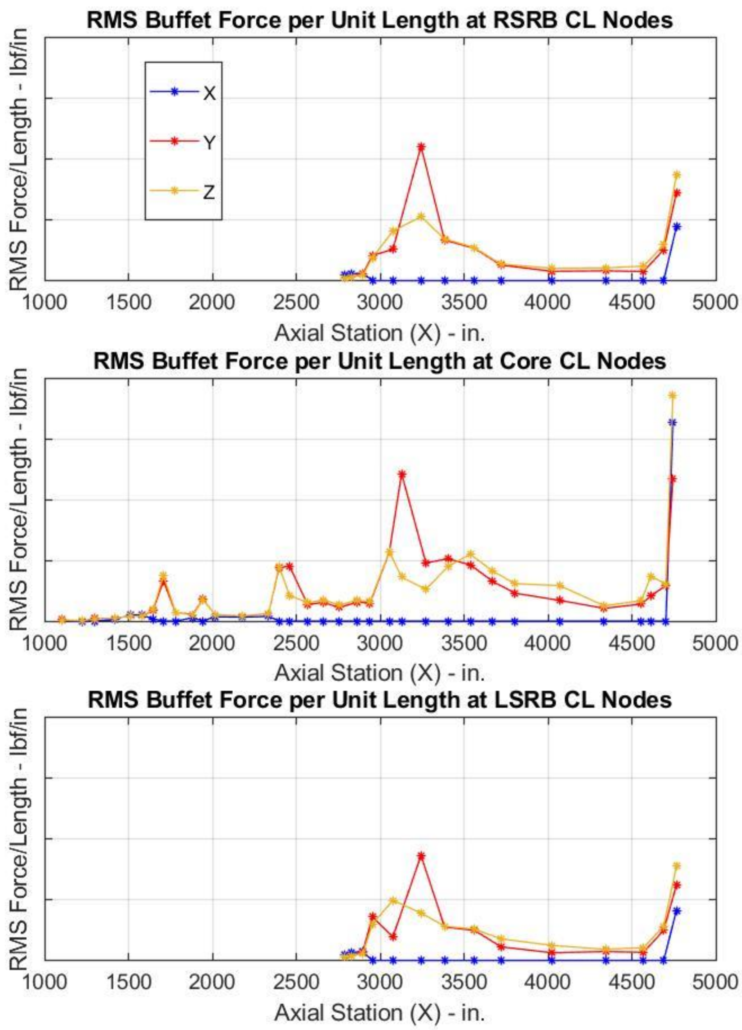

Fig. **2** RMS force per unit length applied at SRB and CS centerline nodes

The Ascent 50 system configuration consists of seven different components: MPCV+MSA, ICPS+LVSA, CS, left (LSRB), right (RSRB), LSRB_CBAR, and RSRB_CBAR. All the components are HCB models except for LSRB_CBAR and RSRB_CBAR, which are simple bar representations of the connections between the boosters and the CS. The Ascent 50 system uncertainty model is based on the component uncertainty models derived for the pretest and updated ICPS/LVSA, which were generated based on the ISPE configuration 3 test-analysis correlation results presented in the previous section. In this buffet UQ analysis, the updated uncertainty model is used for the ICPS/LVSA HCB component. However, there is currently no test-analysis correlation data available for any of the other six components. Therefore, the uncertainty models for these components are based on the two uncertainty models derived for the ICPS/LVSA. The pretest level is based on the ICPS/LVSA pretest uncertainty model and corresponds to the assignment of three bins of frequency uncertainty (1.39%, 9.01%, 10.91%) to the HCB FI modes based on the modes' MEM. The HCB stiffness matrix normalized dispersion is assigned so that the most probable DCGM value based on sweeping the dispersion over a range in a series of MC analyses corresponds to the pretest value of 90.44. This uncertainty model is applied to components that have no heritage and no available modal test-analysis correlation data, such as the MPCV/MSA. The updated uncertainty level is based on the updated ICPS/LVSA uncertainty model. It corresponds to the assignment of three bins of frequency uncertainty (2.04%, 4.83%, 1.97%) to the HCB FI modes based on MEM. The HCB stiffness matrix normalized dispersion is assigned so that the most probable DCGM value corresponds to the updated model value of 95.43. This uncertainty model is applied to components that have a heritage of previous use, testing, and model validation, such as the boosters. Table 2 summarizes the resulting uncertainty models for all seven components based on the two uncertainty levels.

Note that the CS is assigned an updated level of uncertainty, even though the component has no history and the pretest HCB model is being used, because CS mode-shape uncertainty is very sensitive to both the assigned FI eigenvalue uncertainty and the stiffness matrix dispersion. The reduced uncertainty level is assigned to predict what is expected for CS section load uncertainty in the case where the CS model has been updated. The left and right boosters are assigned the same updated-level uncertainty model, even though the HCB representations are slightly different. The two booster CBAR components are relatively simple components; therefore, they are also assigned the updated level of uncertainty, although in this case, a slightly different approach must be taken to assign an uncertainty model. The two components are essentially triaxial springs with twelve rigid body modes and three elastic modes. They are not HCB component representations; therefore, FI eigenvalue uncertainty cannot be assigned. The stiffness dispersion was determined such that the mean RMS uncertainty of the three elastic eigenvalues had a value of 5%, corresponding to the assumed average level of eigenvalue uncertainty over all FI eigenvalues in the updated ICPS/LVSA model.

An MC analysis was performed generating 1000 random system models using the HCB component uncertainty models listed in Table 2. Figure 4 shows the system RMS frequency uncertainty for the first 100 non-slosh elastic modes below 11 Hz. The average RMS uncertainty is 2.75%, with a maximum value of 11.25% for system mode 96. Mode matching between the random and nominal models is not particularly accurate beyond 10 Hz. CS P99 section loads were calculated for each of the 1000 ensemble members using Eq. (31). The corresponding RMS uncertainties in the P99 loads with respect to the nominal section load values are shown in Figure 5. The uncertainty in the CS axial and torsion section loads (X) is much higher than expected, but it is due to variations from relatively small nominal loads forward of the booster-CS connections and at the boattail. The uncertainty in the transverse section shears in the Y direction are also higher than expected between the booster-CS connections, the largest being 26.07% at section X = 4066.86″. While the RMS uncertainty relative to the nominal value is 26.07% for the Y shear force at X = 4066.86″, the standard deviation divided by the mean, or coefficient of variation, is only 4.82%. The large RMS uncertainty is due to a large offset between the nominal value and the mean of the ensemble. Figure 6 shows the P99/90 CS Y shear force compared to the nominal value and the ensemble mean by station. The P99/90 value is determined by computing the 0.90 quantile of the ensemble of random model P99 values. It generally would be expected that the 90th percentile of the P99 ensemble is greater than the nominal model P99 value, but that is not the case because of the large offset between the nominal values and the ensemble means at stations between X = 3125″, where the boosters connect to the CS, and X = 4472″. Large offsets occur at sections with large RMS uncertainty as shown in the top of Figure 6. The same behavior occurs for the CS Z shear forces, but to a lesser extent, as shown in Figure 7.

In contrast, RMS uncertainty in the CS section bending moments in Figure 5 are all less than 10%, except toward the aft end where the moments get smaller. Figure 6 shows a tight dispersion among the nominal P99, P99/90, and mean P99 Z bending moment values. In the region forward of the booster-CS connection, the mean and nominal P99 values are very close, with the P99/90 value being larger as expected. Between the booster-CS connections, the nominal and P99/90 values are very close. Figure 7 illustrates the nominal P99, P99/90, and mean P99 Y bending moment values. In contrast with Z bending moments, the nominal and mean P99 values are very close over almost the entire length of the CS.

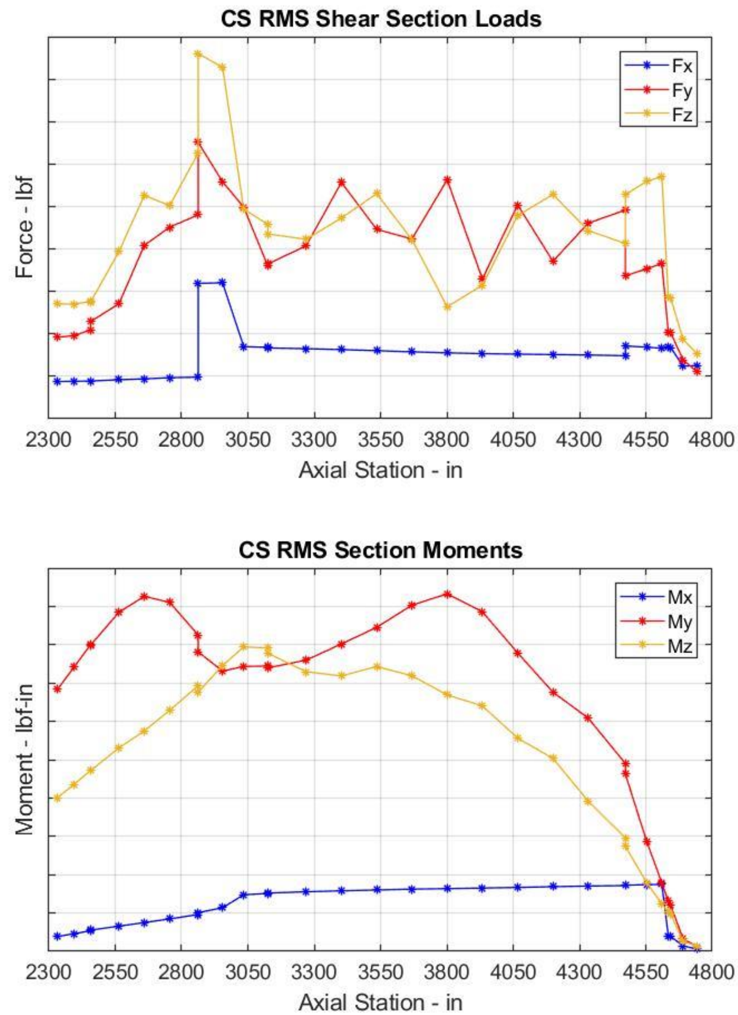

Fig 3 Buffet CS section RMS shear forces and moments

Table 2 Ascent 50 configuration system uncertainty model

Component	Uncertainty Level	Assigned HCB FI Frequency Dispersion	Normalized Stiffness Dispersion
MPCV/MSA	Pretest	1.39%, 9.01%, 10.91%	0.37%
ICPS/LVSA	Updated	2.04%, 4.83%, 1.97%	1.01%
Core	Updated	2.04%, 4.83%, 1.97%	0.30%
LSRB	Updated	2.04%, 4.83%, 1.97%	1.53%
RSRB	Updated	2.04%, 4.83%, 1.97%	1.53%
LSRB CBAR	Updated	0.0%	3.52%
RSRB CBAR	Updated	0.0%	3.52%

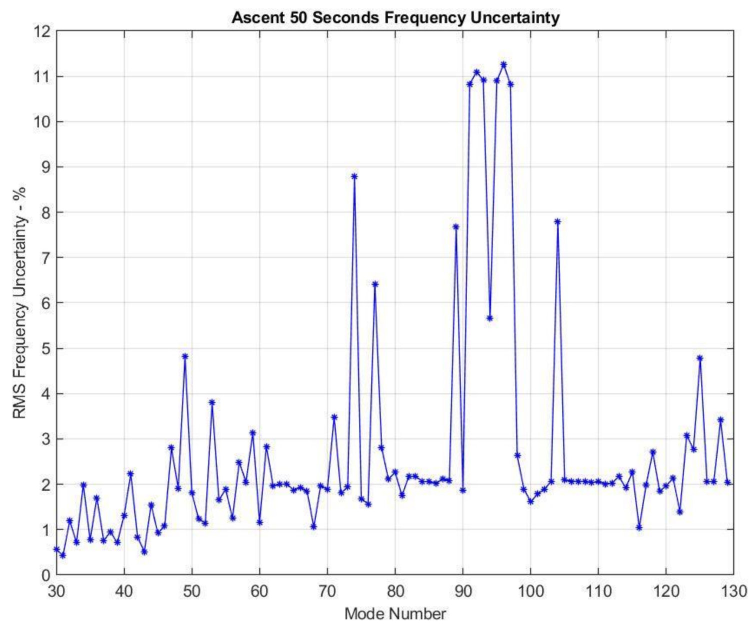

Fig. 4 RMS system frequency uncertainty for non-slosh elastic modes below 11 Hz

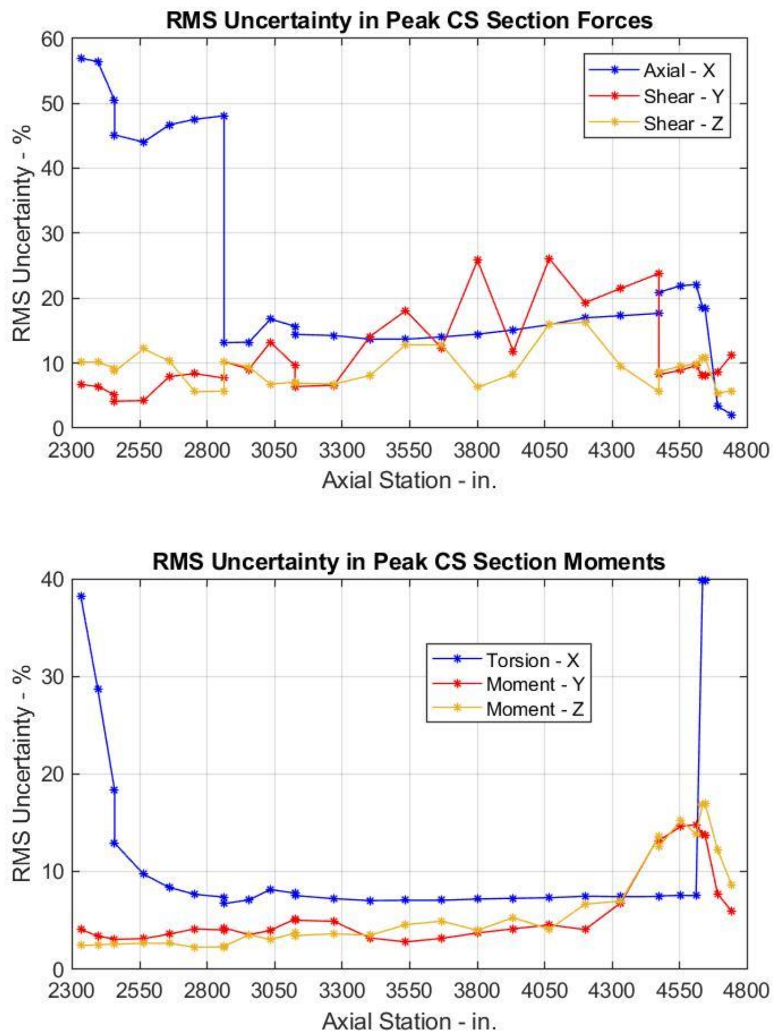

Fig. 5 Percent RMS CS section load uncertainties for Ascent 50 uncertainty model

It was determined that the CS transverse shear forces at sections between the booster and CS connections are very sensitive to uncertainties in the CS HCB FI frequencies. The large offset between the nominal and ensemble mean P99 Y shear forces in Figure 6 is due to modes between 30 and 40 Hz, while the large offset between the nominal and ensemble mean P99 Z shear forces in Figure 7 is due to modes between 15 and 20 Hz. The Y and Z buffet forces with the largest RMS magnitude acting on the core centerline have a significant amount of power in these two frequency regions, respectively. It is believed that the variability of the mode shapes in the 15–20 Hz. and 30–40 Hz. frequency bands due to the uncertainty in the CS HCB FI frequencies causes the RMS response of the transverse shear forces to drop significantly compared to the nominal response, causing large RMS shear force uncertainties relative to the nominal values. This was confirmed by computing the uncertainty in the transverse acceleration frequency response of the CS centerline nodes. While the reduced transverse shear response predicted for the random models within the MC analysis been confirmed using both time- and frequency-domain analysis, the physical cause of the reduced transverse shear response is currently unknown. In contrast, the structurally more significant CS section bending moments are much less sensitive to uncertainty in the CS, leading to reduced uncertainty levels. Future work will further investigate the source and validity of the reduced random response of the CS transverse section loads.

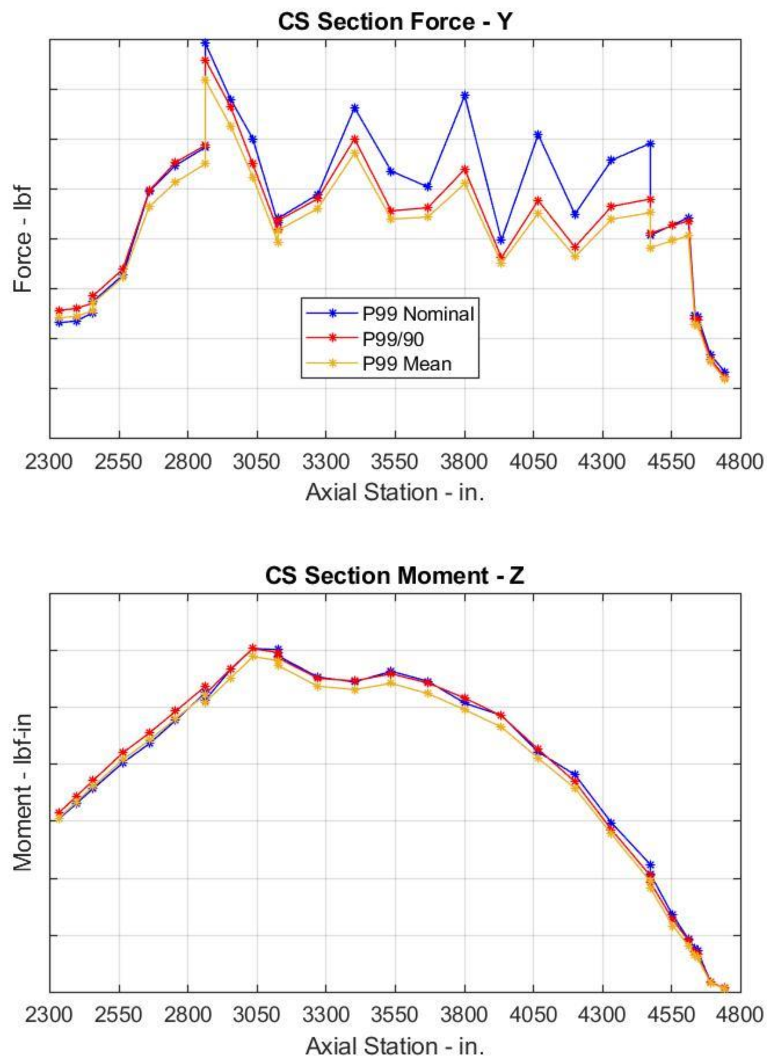

Fig. 6 P99 nominal, mean, and P99/90 CS Y section shears and Z bending moments

CONCLUSION

Uncertainty in structural responses during launch is a significant concern in the development of spacecraft and launch vehicles, where small variations in mode shapes and their interactions can result in significant variation in system loads. CLA, using HCB component models, is the accepted method for determining the response of a launch vehicle/payload system to transient forces, such as liftoff, engine ignitions and shutdowns, jettison events, and atmospheric flight loads, such as buffet. UQ is used to determine statistical bounds on prediction accuracy based on model uncertainty. In this paper it is assumed that the uncertainty is most naturally represented at the component HCB level. In an effort to account for model uncertainties and their effect on CLA predictions, this work combines CLA and UQ in a process termed VCLA. The UQ component is performed using the HPV method, which combines parametric and nonparametric uncertainty at the HCB component model level. The HPV method requires the selection of dispersion values for the HCB FI eigenvalues, and the

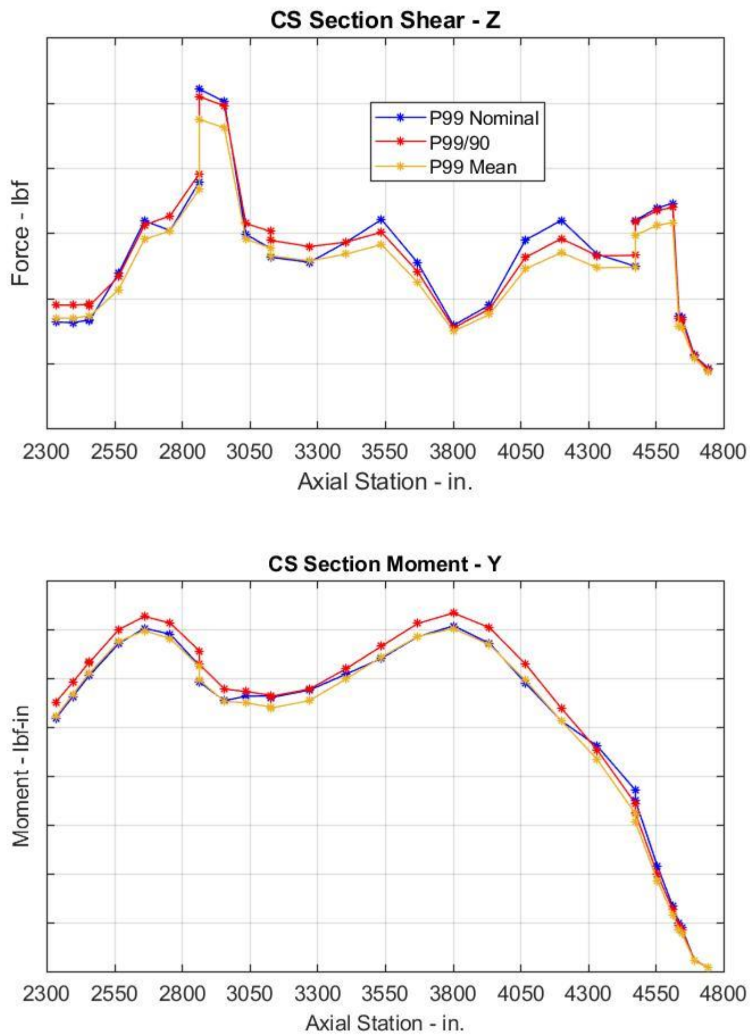

Fig. 7 P99 nominal, mean, and P99/90 CS Z section shears and Y bending moments

HCB mass and stiffness matrices. The dispersions are based on component test-analysis modal correlation results. In the past, there has been a problem of mapping uncertainty in test configuration modes into uncertainty in HCB flight configuration FI modes due to the fact that the boundary conditions for the two configurations are almost never the same. However, the new approach outlined here properly maps the uncertainty by accounting for the differences in the boundary conditions. VCLA has previously not been feasible due to computational expense, but the HPV approach of UQ combined with the use of judiciously selected HCB interfaces makes the VCLA practical within a MC analysis. The proposed methodology was demonstrated by successful application of the process to a buffet loads analysis of the SLS during the transonic regime at 50 seconds after liftoff. CS section shears and moments were recovered, and relevant statistics were computed. The system uncertainty model based on component test-analysis correlation results produces reasonable uncertainty results for the CS section moments. However, the transverse CS section shear loads were very sensitive to the uncertainty in the CS HCB FI frequencies from the standpoint of producing random responses that were significantly below the nominal values. This produced large RMS uncertainties relative to the nominal shear loads. It is believed that this phenomenon is an artifact of the models being used and not a function of the proposed VCLA method, but future work will further investigate the validity of the predicted results.

[1] R. R. Craig and M. C. C. Bampton, "Coupling of Substructures for Dynamic Analysis," *AIAA Journal,* vol. 6, pp. 1313-1319, 1968.

[2] A. Majed, K. Partin, E. Henkel and T. Sarafin, "Variational Coupled Loads Analyses: Reducing Risk in Development of Space-Flight Hardware," *Journal of Spacecraft and Rockets,* vol. 42, no. 1, pp. 98-104, 2005.

[3] D. Kammer, P. Blelloch and J. Sills, "Test-Based Uncertainty Quantification and Propagation Using Hurty/Craig-Bampton Substructure Representations," in *IMAC*, Orlando, FL, 2019.

[4] R. Ghanem and P. Spanos, Stochastic Finite Elements: A Spectral Approach, New York: Springer, 1991.

[5] J. Wishart, "Generalized product moment distribution in samples," *Biometrika,* vol. 20A), no. 1-2, pp. 32-52, 1928.

[6] C. Soize, "A Nonparametric Model of Random Uncertainties for Reduced Matrix Models in Structural Dynamics," *Probabilistic Engineering Mechanics,* vol. 15, no. 3, pp. 277-294, 2000.

[7] C. Soize, "Maximum Entropy Approach for Modeling Random Uncertainties in Transient Elastodynamics," *J. Acoust. Soc. Am.,* vol. 109, no. 5, pp. 1979-1996, 2001.

[8] S. Adhikari, "Generalized Wishart Distribution for Probabilistic Structural Dynamics," *Comput. Mech.,* vol. 45, pp. 495-511, 2010.

[9] S. Adhikari, "Wishart Random Matrices in Probabilistic Structural Mechanics," *J. Eng. Mech.,* vol. 134, no. 12, pp. 1029-1044, 2008.

[10] E. Capiez-Lernout, M. Pellissetti, H. Pradlwarter, G. I. Schueller and C. Soize, "Data and model uncertainties in complex aerospace engineering systems," *J. Sound Vib.,* vol. 295, no. 3-5, p. 923–938, 2006.

[11] M. Pellissetti, E. Capiez-Lernout, r. H. Pradlwarte, C. Soize and G. Schueller, "Reliability analysis of a satellite structure with a parametric and a non-parametric probabilistic model," *Comput. Methods Appl. Mech. Eng.,* vol. 198, no. 2, p. 344–357., 2008.

[12] M. Mignolet, S. C and J. Avalos, "Nonparametric Stochastic Modeling of Structures with Uncertain Boundary Conditions / Coupling Between Substructures," *AIAA J.,* vol. 51, no. 6, p. 1296–1308, 2013.

[13] C. Soize, Uncertainty Quantification: An Accelerated Course with Advanced Applications in Computational Engineering, Springer, 2017.

[14] A. Ben-Israel and T. Greville, Generalized Inverses - Theory and Applications, 2nd ed., New York: Springer, 2003.

[15] A. Kabe, "Time Domain Buffet Loads Analysis," Aerospace Report No. TOR-2007(2207)-6078, El Segundo, CA, 2006.

[16] D. Piatak, M. Sekula, R. Rausch, J. Florance and T. Ivanco, "Overview of the Space Launch System Transonic Buffet Environment Test Program," in *AIAA SciTech*, Kissimmee, FL, 2015.

[17] B. Sako, A. Kabe and S. Lee, "Statistical Combination of Time Varying Loads," *AIAA Journal,* vol. 47, no. 10, pp. 2338-2349, 2009.